crystals

MDPI

Article

Preparation, Thermal Behavior, and Conformational Stability of HMX/Cyclopentanone Cocrystallization

Yuting Tao, Shaohua Jin, Tongbin Wang, Chongchong She, Kun Chen, Junfeng Wang and Lijie Li *

School of Materials Science and Engineering, Beijing Institute of Technology, Beijing 100081, China
* Correspondence: lilijie2003@bit.edu.cn

Abstract: The cocrystallization of 1,3,5,7-tetranitro-1,3,5,7-tetrazolidine (HMX) with cyclopentanone was achieved via a controlled cooling method, followed by comprehensive characterization that confirmed the α-configuration of HMX within the cocrystal. The enthalpy of dissolution of HMX in cyclopentanone was assessed across a range of temperatures using a C-80 Calvert microcalorimeter, revealing an endothermic dissolution process. Subsequently, the molar enthalpy of dissolution was determined, and kinetic equations describing the dissolution rate were derived for temperatures of 303.15, 308.15, 313.15, 318.15, and 323.15 K as follows: $d\alpha/dt = 10^{-2.46}(1-\alpha)^{0.35}$, $d\alpha/dt = 10^{-2.19}(1-\alpha)^{0.79}$, $d\alpha/dt = 10^{-1.76}(1-\alpha)^{1.32}$, $d\alpha/dt = 10^{-1.86}(1-\alpha)^{0.46}$, and $d\alpha/dt = 10^{-2.02}(1-\alpha)^{0.70}$, respectively. Additionally, molecular dynamics (MD) simulations investigated the intermolecular interactions of the HMX/cyclopentanone cocrystallization process, demonstrating a transformation of HMX from β- to α-conformation within the cyclopentanone environment. Theoretical calculations performed at the ωB97XD/6-311G(d,p) level affirmed that α-HMX exhibited stronger binding affinity toward cyclopentanone compared to β-HMX, corroborating experimental findings. A comprehensive understanding of the dissolution behavior of HMX in cyclopentanone holds significant implications for crystal growth methodologies and cocrystallization processes. Such insights are pivotal for optimizing HMX dissolution processes and offer valuable perspectives for developing and designing advanced energetic materials.

Keywords: 1,3,5,7-tetranitro-1,3,5,7-tetrazocane (HMX); HMX/Cyclopentanone cocrystallization; microcalorimeter; enthalpies; dissolution kinetic equation

Citation: Tao, Y.; Jin, S.; Wang, T.; She, C.; Chen, K.; Wang, J.; Li, L. Preparation, Thermal Behavior, and Conformational Stability of HMX/Cyclopentanone Cocrystallization. *Crystals* **2024**, *14*, 711. https://doi.org/10.3390/cryst14080711

Academic Editor: Yael Diskin-Posner

Received: 14 July 2024
Revised: 2 August 2024
Accepted: 5 August 2024
Published: 8 August 2024

1. Introduction

HMX, characterized by its eight-membered ring structure, exhibits notable attributes such as high density, a rapid burst rate, and excellent thermal stability. It is widely employed as a key component in various high-performance plastic-bonded explosives and propellants. Under ambient conditions, HMX has three pure crystalline phases (α, β, and δ) and one hydrate phase (γ) [1–3], of which β-HMX is the most stable crystalline phase at room temperature and atmospheric pressure and belongs to the $P2_1/c$ space group [4]. Previous studies have shown that different crystalline frms of HMX can be obtained by controlling the cooling rate during the solution crystallization process [5]. Notably, β-HMX stabilizes in a chair conformation, known for its energetically favorable properties. In contrast, α, δ, and γ-HMX adopt less stable boat conformations under similar conditions [6].

In 1962, the solvate of HMX with N,N-dimethylformamide (DMF) was discovered [7,8]. To date, dozens of HMX solvate cocrystals have been identified, such as HMX/N-methyl-2-pyrrolidone, HMX/2,4-dinitro-2,4-diazapentane, and HMX/N-methylpyrrolidone [9–12]. The HMX molecules exhibit α-configuration in HMX/DMF solvates [13]. The HMX molecules in HMX/1,2-phenylenediamine, HMX/2-bromoaniline, and HMX/3,4-diamintoluene cocrystals are similar to those of α, δ, and γ-HMX [14]. Moreover, solvate crystallization plays a crucial role in product purification and recycling and provides a safe method for transporting HMX. Despite extensive research by numerous scholars on HMX solvate cocrystals,

significant gaps remain in understanding the mechanisms of cocrystal processes and the molecular structures and intermolecular forces involved in solvate cocrystals. Cyclopentanone is a common raw material in the pharmaceutical and fragrance industries [15], and it performs well as a solvent in the recrystallization of energetic materials. Our experimental work involving the preparation of HMX from cyclopentanone solutions revealed changes in the crystal morphology of HMX and shifts in the conformation of HMX, which often display characteristics of cocrystallization. Therefore, a comprehensive exploration of HMX dissolution dynamics in cyclopentanone is crucial and warrants further investigation. In addition, molecular dynamics has become a powerful simulation technique. Some researchers have utilized molecular dynamics (MD) methods to simulate solubility parameters and explore how different components affect solubility [16–18]. In this study, we employed a C-80 Calvet microcalorimeter to derive kinetic equations for the dissolution of HMX in cyclopentanone. This involves measuring the enthalpy changes associated with HMX dissolution under controlled conditions of 0.1 MPa and temperatures ranging from 303.15 K to 323.15 K. Additionally, we employed molecular dynamics simulations to investigate the dissolution characteristics of HMX in cyclopentanone and the structural and intermolecular interactions involved in its cocrystallization with cyclopentanone. We also examined the effect of cyclopentanone solvent on HMX's conformation and the conformational transitions present in HMX in the condensed state. Such insights are valuable for advancing our understanding of HMX crystallization processes and enhancing its practical applications.

2. Materials and Methods

2.1. Materials

HMX (octahydro-1,3,5,7-tetranitro1,3,5,7-tetrazocine, β-HMX) with purity above 99.5% was provided by Gansu Yinguang Chemical Industry Group Co., LTD (Baiyin, China). Cyclopentanone with a density of 0.9510 g/cm^3 at 298.15 K was supplied by Beijing Mreda Technology Co., LTD (Beijing, China). KCL (cr) (spectral purity) was purchased from Beijing Chemical Reagent Co., LTD (Beijing, China). The water used in these experiments was deionized.

2.2. Preparation of HMX/Cyclopentanone Cocrystalation

The method of cooling down was used to prepare the HMX/cyclopentanone cocrystallization. With stirring, HMX (140 mg) was dissolved in cyclopentanone (2 mL). The solution was heated to 353.15 K to ensure uniform dissolution. Then, the temperature was gradually decreased to 313.15 K at a rate of 0.5 K/min and maintained at 313.15 K for 120 min to facilitate complete precipitation of crystals. These precipitates were subsequently subjected to filtration, purification, and vacuum drying processes.

2.3. Characterization of HMX/Cyclopentanone Cocrystalation

Powder X-ray diffraction (PXRD) was carried out on an Intelligent X-ray diffractometer (D/teX Ultra 250, Smartlab SE, Tokyo, Japan) with Cu-Kβ radiation (40 kV, 50 mA) in the reflection mode, using a step of 0.01° in the step scan mode, ranging from 5° to 90°. The chemical characteristics of pure α-HMX, β-HMX, and HMX/cyclopentanone cocrystallization were investigated by Fourier transform infrared (ALPHA II, BRUKER, Karlsruhe, Germany) spectrometer in the range of 4000~400 cm^{-1}. The thermal characteristics of pure α-HMX, β-HMX, and HMX/cyclopentanone cocrystallization were tested using a Synchronous thermal analyzer (Labsys Evo STA, SETARAM, Lyon, France) heated from 323.15 to 673.15 K at a rate of 10 K/min. The thermal characteristics of pure β-HMX and HMX/cyclopentanone cocrystallization at 10 Mpa were tested using a High-pressure gas adsorption DSC-EGA (sensys, SETARAM, Lyon, France) heated from 323.15 to 773.15 K at a rate of 10 K/min.

2.4. Calorimeter Experiment of HMX in Cyclopentanone

All experiments were conducted utilizing a C-80 Calvet microcalorimeter (SETARAM, Lyon, France), characterized by a sensitivity of 30 μW/mW and a resolution of 0.10 μW. The enthalpy of dissolution of KCl (spectral purity) in distilled water (9.50 mg/2.10 g) was measured at 298.15 K to validate the system's reliability. The determined $\Delta_{diss}H$ value was 17.22 kJ/mol, which closely agrees with the literature value of 17.24 kJ/mol [19]. As a result, the microcalorimeter used to measure enthalpy is reliable.

The enthalpy change associated with the dissolution of HMX in cyclopentanone was investigated across a range of temperatures (303.15, 308.15, 313.15, 318.15, and 323.15 K). To ensure data accuracy, we repeated each temperature measurement three times.

2.5. Computation

We constructed unit cell models using initial β-HMX and α-HMX structures derived from experimental crystal data (CSD code: OCHTET12 for β-HMX; OCHTET for α-HMX) [1]. The geometrical structures of individual molecules were extracted from these unit cells. Subsequently, homodimers and heterodimers of α-HMX with cyclopentanone were constructed based on their optimized structures, employing the ωB97XD [20] functional in conjunction with a 6-311G(d,p) basis set. Stabilization energies in a vacuum were computed using a supramolecular approach and corrected for basis set superposition error (BSSE) using the counterpoise (CP) method introduced by Boys and Bernardi [21]. In solution, the system was modeled using the self-consistent reaction field (SCRF) method with the revised polarized continuum model (PCM). The relative stability of α- and β-HMX molecules in cyclopentanone was investigated by applying the PCM model. All calculations were carried out using the Gaussian09 package [22].

MD simulations were used to investigate the conformational stability of HMX in cyclopentanone. The reflective index *n* of the cyclopentanone solvent was 1.435, the dielectric constant ε was 13.520, and the density was 0.944 g/cm^3 (298.15 K). The Amorphous Cell tool constructed different cubic boxes. Before the kinetic simulations, the cubic boxes were subjected to energy minimization. The NVT ensemble with periodic boundary conditions, the Andersen temperature control method, and the COMPASS force field approach were used in the simulations. All the simulations in this work are performed using the Materials Studio 2018 software package [23].

3. Results and Discussion

3.1. Crystal Morphology of HMX/Cyclopentanone Cocrystallization

Figure 1 shows optical micrographs of HMX and HMX/cyclopentanone cocrystallization raw materials. As shown in Figure 1a, the raw material HMX is granular crystals with diameters between 50 and 150 μm. As shown in Figure 1b–d, the morphology of HMX/cyclopentanone cocrystallization differs from that of the raw material in that the cocrystals were rod-like crystals with diameters of about 200 μm and most of them were clustered. This difference in morphology indicates that cyclopentanone, as a solvent for the crystallization of HMX, induces a significant alteration in crystal morphology.

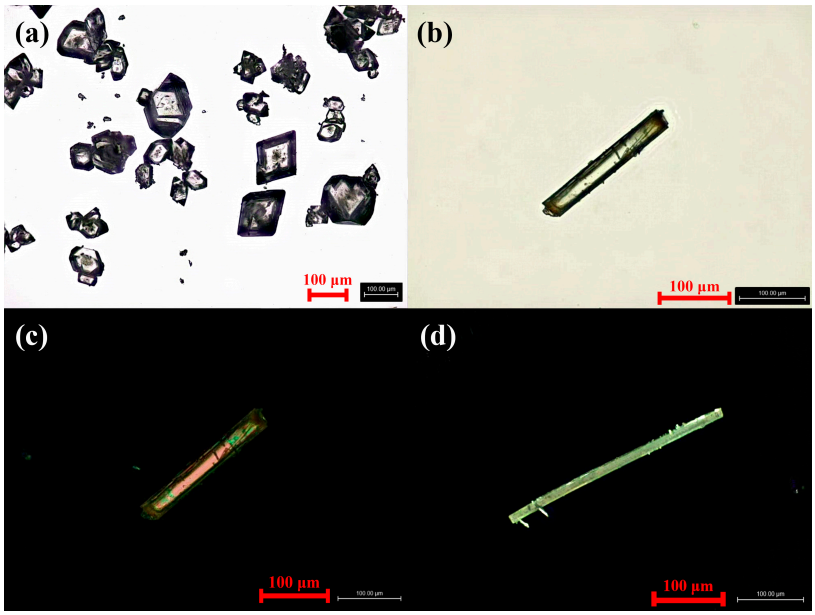

Figure 1. Optical microscope images of (**a**) raw HMX and (**b**) HMX/cyclopentanone cocrystallization and (**c**,**d**) polarized microscope images of HMX/cyclopentanone cocrystallization.

3.2. Chemical Characterization of HMX/Cyclopentanone Cocrystallization

Figure 2 shows the results of the characterization of the crystal forms of β-HMX, α-HMX, raw-HMX, and HMX/cyclopentanone cocrystallization.

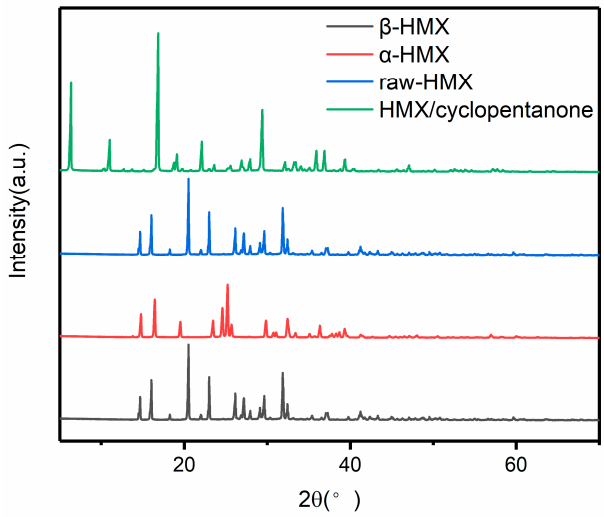

Figure 2. XRD patterns of pure β-HMX, α-HMX, raw-HMX, and HMX/cyclopentanone cocrystallization.

In Figure 2, The strong peaks at 2θ = 14.68°, 20.51°, 23.00°, and 31.86° of β-HMX and those at 2θ = 14.79°, 24.59°, and 25.22°of pure α-HMX vanished from the HMX/cyclopentanone cocrystallization pattern. In its place, the new strong peaks developed at 2θ = 6.36°, 11.01°, 16.83°, 22.11°, and 29.39°. The XRD patterns of HMX/cyclopentanone cocrystallization exhibited distinct differences from those of β- and α-HMX, indicating the formation of a novel crystal form or cocrystal when HMX was crystallized in cyclopentanone.

The infrared spectral curves of the compounds of pure β-HMX, α-HMX, raw-HMX, cyclopentanone, and HMX/cyclopentanone cocrystallization are shown in Figure 3. The results in Figure 3 showed that the raw-HMX is β-HMX, and the crystals precipitated from cyclopentanone were HMX/cyclopentanone cocrystallization. Additionally, Figure 3 shows that, albeit with some changes, the FT-IR spectra of the HMX/cyclopentanone cocrystallization are similar to those of pure α-HMX and cyclopentanone, indicating that

HMX exists in a form similar to the α-conformation in the cocrystal. Among them, the spectrum of HMX's C-H stretching vibration peak is 3035.50 cm^{-1}. However, the C-H stretching vibration of the cocrystal was shifted to 3064.20 cm^{-1}. The ring vibration of the eight-membered ring was displaced from 962.50 cm^{-1} and 937.80 cm^{-1} of β-HMX to 904.90 cm^{-1}. Therefore, after the HMX/cyclopentanone cocrystallization formed, the electron cloud density of the eight-membered ring in the molecular structure of HMX decreased, and the electron cloud density of the C-H bond on the ring increased. Moreover, the C=O stretching bands of cyclopentanone appeared at 1731.60 cm^{-1} while the C=O stretching bands of the cocrystallization were displaced to 1719.20 cm^{-1}, suggesting that the formation of the HMX/cyclopentanone cocrystallization decreases the density of the electron cloud on the carbonyl group of cyclopentanone. Changes in the FT-IR spectra are attributed to hydrogen-bonding interactions between HMX and cyclopentanone molecules in the cocrystallization. Among them, the displacement of the carbonyl characterization peak of cyclopentanone indicates that the hydrogen bonding interaction of the HMX/cyclopentanone cocrystals occurs between the -CH_2 group on the eight-membered ring of HMX and the carbonyl group of cyclopentanone.

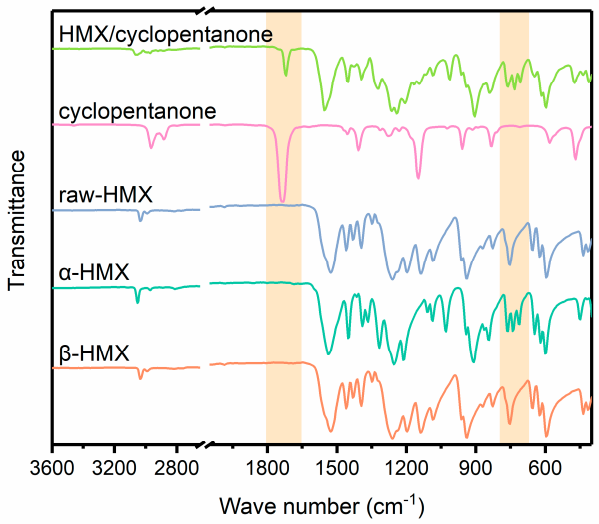

Figure 3. FT−IR spectra of the raw materials and the cocrystallization.

Figure 4 depicts the TG−DTG curves of HMX/cyclohexanone cocrystallization at a heating rate of 10 K/min. The boiling point of pure cyclohexanone is 403.15 K, but due to its complexation with HMX, the boiling point of cyclohexanone is significantly lowered during the thermal decomposition process of the cocrystallization. According to Figure 4, the thermal decomposition of HMX/cyclohexanone can be primarily divided into solvent evaporation and HMX decomposition stages. Therefore, the mass loss of the HMX/cyclohexanone cocrystallization is primarily caused by the evaporation of cyclohexanone and the decomposition of HMX. Through calculations, it has been determined that the mass contents of HMX and cyclohexanone in the cocrystal are 48.96% and 14.68%, respectively, indicating a molar ratio of 1:1 between them.

As shown in Figure 5, the DSC curves further demonstrate the production of HMX/cyclopentanone cocrystallization. The endothermic peak at 367.70 K was mainly due to the decomposition of the supramolecular structure of HMX/cyclopentanone, the breakdown of weak interaction forces such as hydrogen bonding in the supramolecular compound, and the solvent molecules of cyclopentanone were removed in a gaseous state. For pure β-HMX, the endothermic peak at 461.48 K corresponds to the transition peak of $\beta \rightarrow \delta$, while the melting peak occurs at 550.37 K, and the exothermic decomposition peak is at 554.57 K. As for pure α-HMX, the endothermic peak at 489.38 K represents the transition peak of $\alpha \rightarrow \delta$, with the melting peak at 550.15 K and the exothermic decomposition peak at 554.49 K. Comparing HMX/cyclohexanone cocrystallization with the

pure phases shows that the melting point (T_m) and decomposition temperature (T_p) of HMX/cyclohexanone cocrystallization are nearly identical to those of pure HMX particles. This indicates that cyclohexanone does not affect the non-isothermal stability of HMX in the HMX/cyclohexanone cocrystal. Meanwhile, we analyzed the enthalpies of the decomposition peaks of HMX/cyclohexanone, β-HMX, and α-HMX, which were 1143.61 J/g, 1442.41 J/g, and 1375.82 J/g, respectively. Combined with Figure 4, the molar ratio of HMX and cyclohexanone in HMX/cyclohexanone cocrystals was 1:1, and the theoretical enthalpy value, if the component HMX were completely decomposed, would be 1468.43 J/g, while the actual enthalpy of the cocrystallization is lower than the theoretical value, indicating an interaction between cyclopentanone and HMX. Moreover, the HMX/cyclopentanone desolvation showed the same thermal characteristics as that of β-HMX, which is consistent with the literature reports [11].

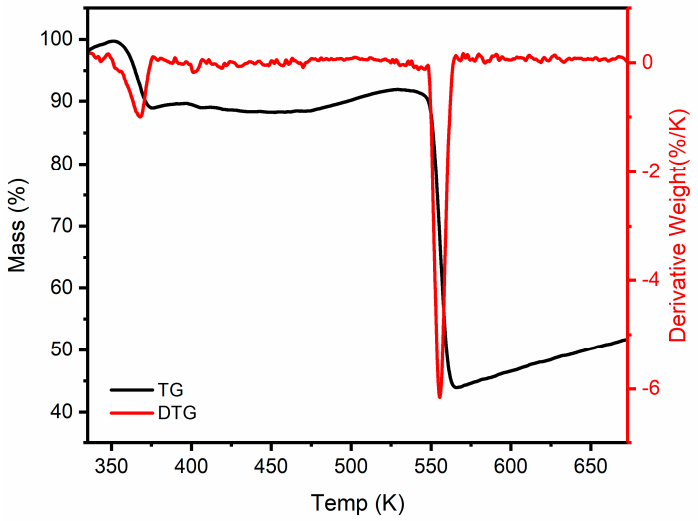

Figure 4. TG−DTG curves of HMX/cyclopentanone cocrystallization.

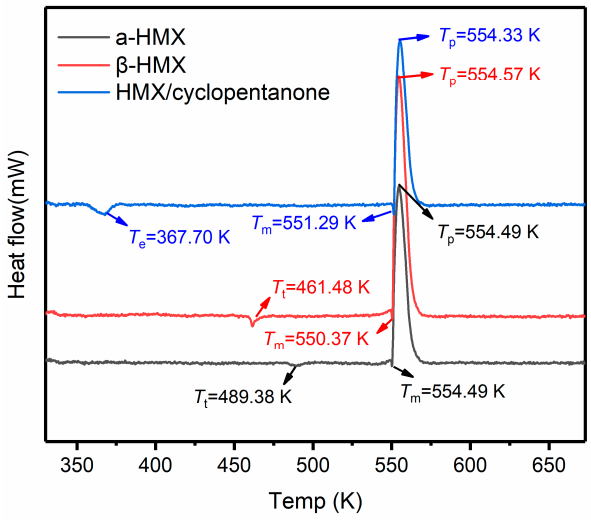

Figure 5. DSC curves of pure β-HMX, α-HMX, and HMX/cyclopentanone cocrystallization.

Figure 6 depicts the high-pressure DSC curves of HMX and HMX/cyclopentanone cocrystallization at 10 MPa. The decomposition peak temperatures of HMX and HMX/cyclopentanone cocrystallization are nearly identical, suggesting that their non-isothermal stability is essentially equivalent. In addition, under high pressure, the second decomposition exothermic peak appeared in HMX, which showed obvious autocatalytic and autothermal phenomena, while HMX/cyclopentanone cocrystallization did not have such phenomena.

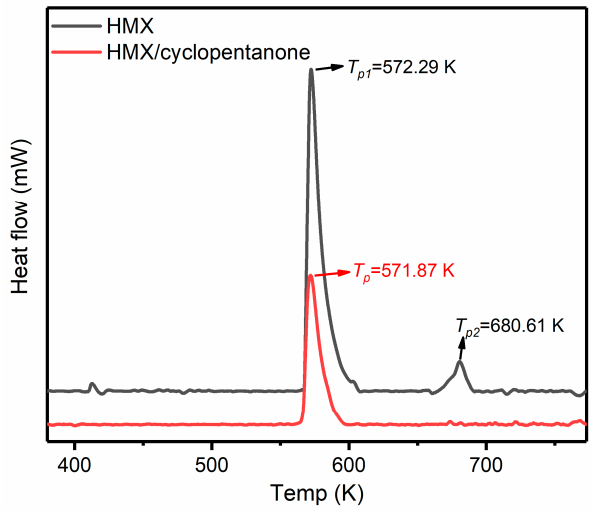

Figure 6. High-pressure DSC curves of pure β-HMX and HMX/cyclopentanone cocrystallization.

3.3. Thermochemical Behavior of HMX in Cyclopentanone

Temperature significantly influences the formation of cocrystals. Therefore, comprehending the solubility properties of HMX in cyclopentanone is essential for the efficient preparation of HMX/cyclopentanone cocrystallization. The dissolution processes for HMX in cyclopentanone are endothermic, as can be observed from the heat flow curve of HMX dissolution in Figure 7. In addition, it can be seen from Figure 7 that the heat absorbed by the dissolution process of HMX in cyclopentanone increases and then decreases as the temperature increases, with the most heat absorbed at 313.15 K. Table 1 lists the experimental values of heat changes for the dissolution of HMX in cyclopentanone across varying temperatures, alongside the corresponding molar enthalpies ($\Delta_{diss}H$) for each process. Here, a is the amount of the substance, b is the molar concentration of the solution, and Q is the heat effect generated during the dissolution. Because of the solution's low molar concentration, the molar enthalpy of an infinitely dilute solution can be expressed using the value of $\Delta_{diss}H$.

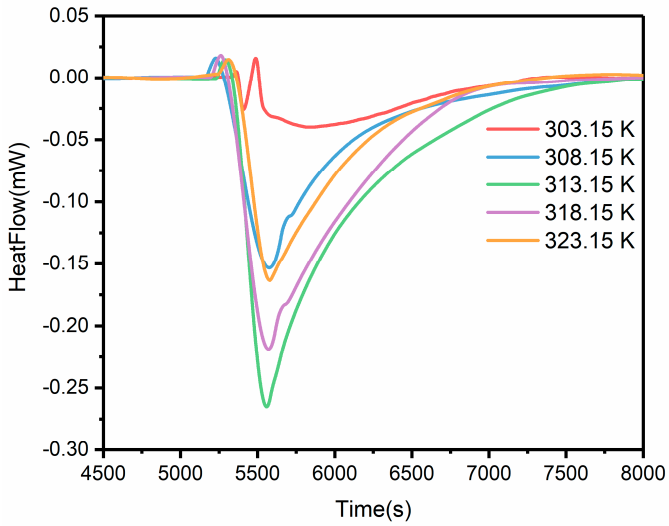

Figure 7. The curve of heat−flow of HMX in cyclopentanone.

Table 1. HMX dissolution enthalpies at different temperatures at 0.1 MPa pressure in cyclopentanone.

T (K)	$10^6 \times$ a (mol)	$10^2 \times$ b (mol/L)	Q (J)	$\Delta_{diss}H$ (kJ/mol)
303.15	8.71	0.87	0.0915	10.50
308.15	9.52	0.95	0.1046	10.98
313.15	9.72	0.97	0.1868	19.21
318.15	9.35	0.94	0.1496	16.00
323.15	8.67	0.86	0.1047	12.11

During the dissolution of substances, two concurrent processes are typically observed: firstly, solute particles detach from the solid surface and diffuse into the solvent, absorbing heat; secondly, solute particles interact with solvent molecules to form solvent compounds, accompanied by heat release. The heat absorbed and released is not equal for different solutes and solvents. As shown in Table 1, the thermal effect produced by cyclopentanone during HMX dissolution increases and then decreases with increasing temperature, reaching its highest value at 313.15 K. This may be because HMX is more susceptible to forming solvent compounds when the temperature reaches 313.15 K and above.

3.4. Kinetics of the Dissolution Process

The kinetic Equations (1) and (2) are selected as model functions to explain how HMX dissolves in cyclopentanone [13,24–26]:

$$\frac{da}{dt} = kf(a), \tag{1}$$

$$f(a) = (1-a)^n, \tag{2}$$

Combining Equations (1) and (2) yields Equation (3)

$$\frac{da}{dt} = k(1-a)^n, \tag{3}$$

Substituting the $a = H/H_\infty$ [27] into Equation (3), we get:

$$ln\left[\frac{1}{H_\infty}\left(\frac{dH}{dt}\right)_i\right] = ln\,k + nln\left[1-\left(\frac{H}{H_\infty}\right)_i\right] \; i = 1, 2, \cdots, L \cdots, \tag{4}$$

where a is the conversion degree, H is the enthalpy at the time of t, H_∞ is the enthalpy of the whole dissolution process, k is the rate constant for the dissolution of HMX in cyclopentanone, and n is the number of reaction stages. Table A1 lists the raw data of HMX dissolved in cyclopentanone at five temperatures. By substituting the raw data of Table A1 into the kinetic Equation (4), the values of n and *lnk* are obtained at different temperatures and are listed in Table 2.

Table 2. The values of *n* and *lnk* for the dissolution process at different temperatures.

T (K)	*n*	*lnk*	*r*
303.15	0.3549	−5.6641	0.9940
308.15	0.7911	−5.0505	0.9940
313.15	1.3185	−4.1569	0.9935
318.15	0.4623	−4.2205	0.9901
323.15	0.7517	−4.2940	0.9947

As demonstrated in Table 2, the varying values of *n* and *lnk* show that the number of reaction orders and the rate of HMX dissolution in cyclopentanone varied as the experiment temperature changed. At 303.15–313.15 K, *lnk* slightly increased, and at 313.15–323.15 K, *lnk* slightly decreased.

At various temperatures, the dissolving kinetic equations of HMX in cyclopentanone are described by applying Equations (A1)–(A5), see Appendix A. Equation (5) is utilized as a model function to depict the rate at which HMX dissolves in cyclopentanone [28].

$$ln\ k = ln\ A - \frac{E}{RT}, \tag{5}$$

Based on Equation (5) and Figure 8, the values of E and lnA for the dissolution process in the temperature range of 303.15–313.15 K were 118.82 kJ/mol and 41.43, respectively, and the values of E and lnA for the dissolution process in the temperature range of 313.15–323.15 K were −11.53 kJ/mol and −8.28, respectively. The results showed that the dissolution process could occur readily between 313.15 K and 323.15 K. The complex between HMX and cyclopentanone was more likely to form at temperatures higher than 313.15 K.

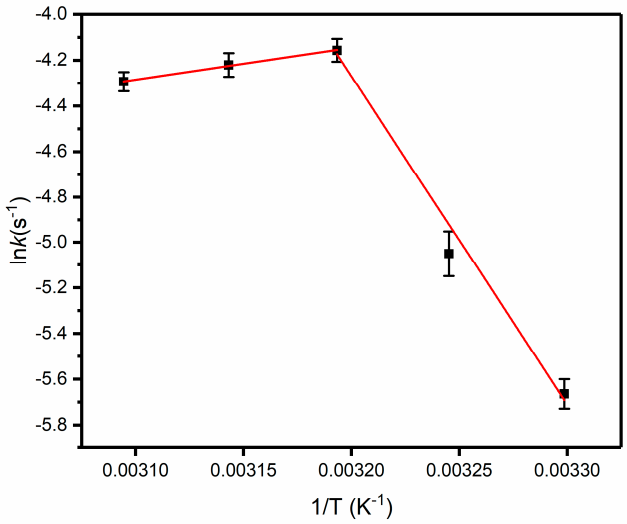

Figure 8. The relationship of reaction rate constant (k) versus temperature (T) for the dissolution of HMX in cyclopentanone (the red line is the best−fit line).

3.5. Conformation Stability of HMX Molecule in Cyclopentanone

The thermal effect of the dissolution process for β-HMX in cyclopentanone first increases and then decreases with increasing temperature, reaching its highest value at 313.15 K. Thus, based on the experiment, the simulation temperature was set at 313.15 K, and a β-HMX molecule was placed in the simulation box that had 200 cyclopentanone molecules (atoms totaling 2828) to create the theoretical model for MD simulation. Cyclopentanone molecules initially surrounded the HMX molecule at random. The trajectories were gathered for further analysis at 500 fs intervals, with a time step of 1 fs and a period of 1 ns. As depicted in Figure 9, the HMX molecule transforms over time. Previous studies have shown that the molecular conformations of the four crystalline types (α, β, γ, and δ crystalline types) of HM X are different: α-HMX is a boat-shaped molecular conformation with a double axis of symmetry; β-HMX has a chair-shaped molecular conformation with one center of symmetry [29]; and the molecular conformations of γ-HMX and δ-HMX are similar to those of α-HMX molecules but do not have a perfect double symmetry [30]. The simulation results showed that the HMX molecules exhibited the characteristics of secondary axial symmetry under the action of cyclopentanone, so it can be indicated that the transition from β-HMX to α-HMX occurred under this action. Initially, at 0 ps, the HMX molecule was optimized to exhibit characteristics of the β-configuration predominantly. As time progressed, under the influence of solvent molecules, the configuration of the HMX molecule gradually transitioned toward the α-configuration. By 670 ps, the β-HMX molecule had transformed into the α-configuration.

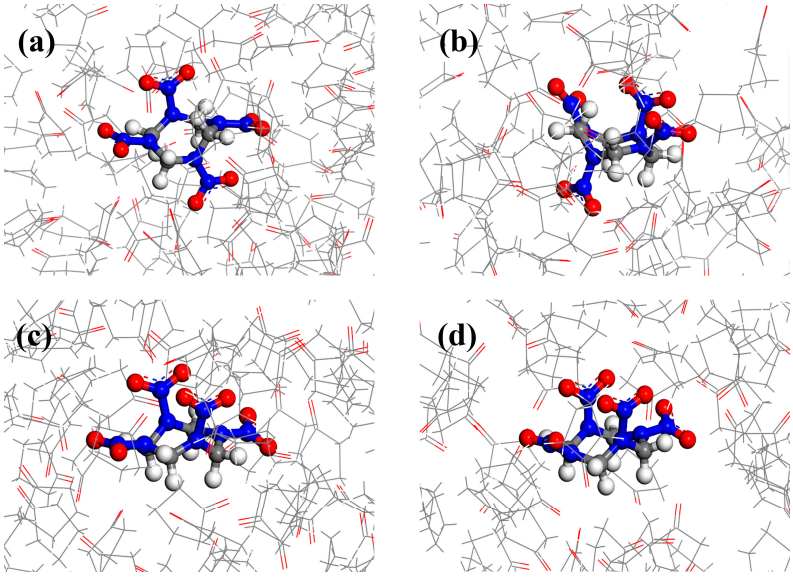

Figure 9. Screenshots of MD simulations of HMX in cyclopentanone at 313.15 K: (**a**) 0 ps; (**b**) 345 ps; (**c**) 666 ps; and (**d**) 670 ps. (HMX molecules are represented by a ball-and-stick, and cyclopentanone molecules are represented by a line.).

The relative stability of HMX molecule conformations in cyclopentanone was explicated via the computation of binding energies between distinct HMX conformations and the adjacent cyclopentanone molecules. The cubic box containing 200 cyclopentanone molecules and one β- or α-HMX molecule was optimized using molecular mechanics methods to calculate the binding energy between cyclopentanone and HMX. For β-HMX and α-HMX, the calculated binding energies were 50.38 kcal/mol and 53.54 kcal/mol, respectively. The electrostatic interaction energy between α-HMX and cyclopentanone was 23.65 kcal/mol, and that between β-HMX and cyclopentanone was 20.01 kcal/mol. The results showed that the electrostatic interaction between α-HMX and cyclopentanone molecules was stronger than that between β-HMX and cyclopentanone molecules. Additionally, quantum chemistry simulations were carried out to investigate the relative stability of the HMX molecule configuration in cyclopentanone further. The total molecular energies of α-HMX and β-HMX under vacuum conditions were calculated at the ωB97XD/6-311G(d,p) level, where the total energy of β-HMX molecules was 2.47 kcal/mol lower than that of α-HMX. The PCM model treated solvent effects. Following PCM correction, the total energy of an α-HMX molecule was 0.96 kcal/mol lower than that of a β-HMX molecule at the ωB97XD/6-311G(d,p) level. In addition, the total energy of both α-HMX and β-HMX molecules in the presence of cyclopentanone is lower than their total molecular energy under vacuum conditions, and the total molecular energy of α-HMX is lower.

Based on the aforementioned results, it can be inferred that dissolving solid β-HMX in cyclopentanone solvent leads to its conversion into α-HMX over time. This is consistent with experimental observations of α-HMX predominance in the HMX/cyclopentanone cocrystallization. From a molecular geometry perspective, both α-HMX and cyclopentanone exhibit strong polarity, whereas β-HMX is relatively nonpolar. Therefore, the solvent's preference for polar conformations may be the reason for the significant stability of α-HMX in cyclopentanone.

To explore the possibility of α-HMX cocrystallizing with cyclopentanone, homodimers and heterodimers of α-HMX were studied. The structures of all possible dimers were constructed according to the possible mode of interaction. All structures were optimized using the ωB97XD/6-311G(d,p) level. The most stable configurations obtained are shown in Figure 10, and the corresponding stabilization energies are given in Table 3. According to calculations incorporating basis set superposition error (BSSE) correction, the stabilization

energies of the α-HMX/cyclopentanone heterodimer exceeded those of the cyclopentanone homodimer and were comparable to those of the α-HMX homodimer. As shown in Figure 10, C-H···O hydrogen bonding interactions exist in all dimers. Among them, for the α-HMX/cyclopentanone dimer, a pyramidal hydrogen bonding network was formed mainly between the four methylene H atoms of α-HMX and the carbonyl O atoms of cyclopentanone, with bond lengths of 2.35, 2.32, 2.34, and 2.35 Å, respectively. The simulation results agree with the experimental FT-IR spectroscopy studies that C-H···O hydrogen bonding enables α-HMX to build a 1:1 complex with cyclopentanone.

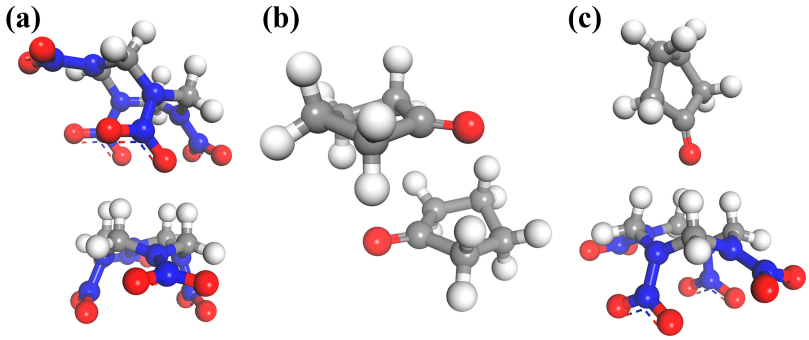

Figure 10. α-HMX and cyclopentanone dimer structures optimized at the ωB97XD/6-311G(d,p) level ((**a**) α-HMX/α-HMX; (**b**) cyclopentanone/cyclopentanone; (**c**) α-HMX/cyclopentanone).

Table 3. The raw data of the dissolution of HMX at different temperatures at 0.1 MPa pressure in cyclopentanone.

	E_{tot} (a.u.)	ΔE_s [1] (kcal/mol)	E_{BSSE} [2] (kcal/mol)	$\Delta E'_s$ [3] (kcal/mol)
α-HMX/cyclopentanone	−1467.05	−14.04	2.29	−11.75
α-HMX dimer	−2392.99	−16.45	3.15	−13.30
Cyclopentanone dimer	−541.12	−9.73	2.24	−7.49

[1] Energies of stabilization without BSSE adjustment. [2] BSSE correction energies. [3] BSSE-corrected stabilization energies at the ωB97XD/6-311G(d,p) level.

Figure 11 displays the equilibrium molecular dynamics simulation results of HMX in a cyclopentanone environment, revealing C-H···O hydrogen bonding interactions between α-HMX and cyclopentanone. These interactions suggest a potential mechanism wherein the hydrogen-bonded structure between HMX and cyclopentanone facilitates the transformation of β-HMX to α-HMX, culminating in the formation of the α-HMX/cyclopentanone cocrystallization.

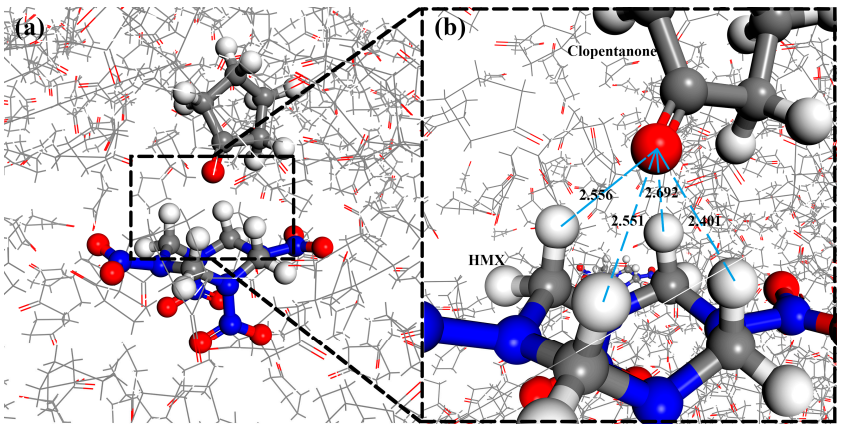

Figure 11. (**a**) Final structures after equilibrated for by after molecular dynamics simulation; (**b**) Interaction of HMX with cyclopentanone (The dashed line indicates the distance between the O atom of the cyclopentanone carbonyl and the four methylene H atom of HMX in Å).

4. Conclusions

In this work, we have investigated HMX/cyclopentanone cocrystallization mainly experimentally and theoretically. The main findings can be summarized as follows:

(1) HMX/cyclopentanone cocrystallization was synthesized using a cooling method, and their structures and properties were characterized using PXRD, FT−IR, TG−DSC, and high-pressure DSC techniques. The results indicated the formation of cocrystals at 313.15 K with a 1:1 molar ratio, wherein HMX adopted the α-configuration.

(2) The dissolution behavior of HMX in cyclopentanone was investigated. The results showed that the heat absorbed during the dissolution of HMX by cyclopentanone increased and then decreased with increasing temperature, reaching a maximum of 313.15 K. HMX is more likely to form cocrystallization with cyclopentanone when the temperature reaches 313.15 K and above. The enthalpies of dissolution of HMX in cyclopentanone solvent at five temperature points and the dissolution kinetic equations were also obtained.

(3) The structural and intermolecular interactions governing the cocrystallization of HMX with cyclopentanone were investigated via molecular dynamics (MD) simulations. The findings reveal an intensified binding affinity between α-HMX and cyclopentanone solvent molecules, facilitating the transition of HMX from its β- to α-configuration, consistent with experimental observations. Quantum chemical calculations conducted at the ωB97XD/6-311G(d,p) level further affirm the greater stability of α-HMX over β-HMX within the cyclopentanone solvent, evidenced by lower total molecular energy. The predominant intermolecular forces identified in this context predominantly involve C-H$\cdots$O hydrogen bonding interactions.

Author Contributions: Conceptualization, Y.T., S.J. and L.L.; preparation and dissolution experiments, Y.T.; high-pressure DSC experiment, T.W.; guidance for calculations, C.S.; data curation, Y.T.; writing—original draft preparation, Y.T.; writing—review and editing, Y.T., K.C., J.W. and L.L.; supervision, L.L. All authors have read and agreed to the published version of the manuscript.

Funding: This research received no external funding.

Data Availability Statement: The data presented in this study are available on request from the corresponding author.

Acknowledgments: The authors are grateful to the editor and three anonymous reviewers for their comments, which have greatly improved the quality of this manuscript.

Conflicts of Interest: The authors declare no conflicts of interest.

Appendix A

Table A1. The raw data of the dissolution of HMX at different temperatures at 0.1 MPa pressure in cyclopentanone.

T (K)	m (mg)	t (s)	$-(dH/dt)_i$ (mJ/s)	$(H/H_\infty)_i$	$-H_\infty$ (kJ/mol)
303.15	2.58	200	−0.0289	0.1277	10.5044
		400	−0.0315	0.2932	
		600	−0.0300	0.4515	
		800	−0.0269	0.5931	
		1000	−0.0235	0.7119	
		1200	−0.0200	0.8051	
		1400	−0.0174	0.8768	
308.15	2.82	200	−0.0561	0.2833	10.9809
		400	−0.0405	0.5069	
		600	−0.0293	0.6591	
		800	−0.0210	0.7629	
		1000	−0.0168	0.8364	
		1200	−0.0129	0.8899	
		1400	−0.0103	0.9293	

Table A1. *Cont.*

T (K)	m (mg)	t (s)	$-(dH/dt)_i$ (mJ/s)	$(H/H_\infty)_i$	$-H_\infty$ (kJ/mol)
313.15	2.88	200	0.1960	0.2295	18.8202
		400	0.1291	0.4536	
		600	0.0832	0.6144	
		800	0.0551	0.7329	
		1000	0.0328	0.8213	
		1200	0.0187	0.8868	
		1400	0.0068	0.9352	
318.15	2.77	200	0.2192	0.2527	15.8023
		400	0.1753	0.4945	
		600	0.1350	0.6775	
		800	0.1016	0.8112	
		1000	0.0727	0.9030	
		1200	0.0503	0.9595	
		1400	0.0324	0.9884	
323.15	2.56	200	0.1416	0.2280	11.9946
		400	0.1041	0.4934	
		600	0.0687	0.6831	
		800	0.0433	0.8098	
		1000	0.0278	0.8922	
		1200	0.0183	0.9456	
		1400	0.0097	0.9793	

By entering the values from Table 2 into Equation (3), the corresponding kinetic equations that describe the dissolution rate at the five experimental temperatures:

$$\frac{da}{dt} = 10^{-2.46}(1-a)^{0.35} \quad T = 303.15\ K, \tag{A1}$$

$$\frac{da}{dt} = 10^{-2.19}(1-a)^{0.79} \quad T = 308.15\ K, \tag{A2}$$

$$\frac{da}{dt} = 10^{-1.76}(1-a)^{1.32} \quad T = 313.15\ K, \tag{A3}$$

$$\frac{da}{dt} = 10^{-1.86}(1-a)^{0.46} \quad T = 318.15\ K, \tag{A4}$$

$$\frac{da}{dt} = 10^{-2.02}(1-a)^{0.70} \quad T = 323.15\ K, \tag{A5}$$

References

1. Cady, H.H.; Larson, A.C.; Cromer, D.T. The Crystal Structure of α-HMX and a Refinement of the Structure of β-HMX. *Acta Crystallogr.* **1963**, *16*, 617–623. [CrossRef]
2. Cobbledick, R.E.; Small, R.W.H. The crystal structure of the δ-form of 1,3,5,7-tetranitro-1,3,5,7-tetraazacyclooctane (δ-HMX): Erratum. *Acta Crystallogr. Sect. B* **1975**, *31*, 332. [CrossRef]
3. Main, P.; Cobbledick, R.E.; Small, R.W.H. Structure of the fourth form of 1,3,5,7-tetranitro-1,3,5,7-tetraazacyclooctane (γ-HMX), $2C_4H_8N_8O_8.0.5H_2O$. *Acta Crystallogr.* **1985**, *41*, 1351–1354. [CrossRef]
4. Gao, D.; Huang, J.; Lin, X.; Yang, D.; Wang, Y.; Zheng, H. Phase transitions and chemical reactions of octahydro-1,3,5,7-tetranitro-1,3,5,7-tetrazocine under high pressure and high temperature. *RSC Adv.* **2019**, *9*, 5825–5833. [CrossRef] [PubMed]
5. McCrone, W.C. CRYSTALLOGRAPHIC DATA. 36. Cyclotetramethylene Tetranitramine (HMX). *Anal. Chem.* **1950**, *22*, 1225–1226. [CrossRef]
6. Brill, T.B.; Reese, C.O. Analysis of intra- and intermolecular interactions relating to the thermophysical behavior of .alpha.-, .beta.-, and .delta.-octahydro-1,3,5,7-tetranitro-1,3,5,7-tetraazocine. *J. Phys. Chem.* **1980**, *84*, 1376–1380. [CrossRef]
7. Bedard, M.; Huber, H.; Myers, J.L.; Wright, G.F. The Crystalline Form of 1,3,5,7-Tetranitro-1,3,5,7-tetrazacyclooctane (HMX). *Can. J. Chem.* **1962**, *40*, 2278–2299.
8. Cobbledick, R.E.; Small, R.W.H. The crystal structure of the complex formed between 1,3,5,7-tetranitro-1,3,5,7-tetraazacyclooctane (HMX) and N,N-dimethylformamide (DMF). *Acta Crystallogr. Sect. B* **1975**, *31*, 2805–2808. [CrossRef]

9. Haller, T.M.; Rheingold, A.L.; Brill, T.B. Structure of the 1/1 complex between octahydro-1,3,5,7-tetranitro-1,3,5,7-tetrazocine (HMX), C4H8N8O8, and N-methyl-2-pyrrolidinone (NMP), C5H9NO. *Acta Crystallogr. Sect. C* **1985**, *41*, 963–965. [CrossRef]
10. Liu, Y.; Xu, J.; Huang, S.; Li, S.; Wang, Z.; Li, J.; Jia, J.; Huang, H. Microstructure and performance of octahydro-1,3,5,7-tetranitro-1,3,5,7-tetrazocine (HMX) crystal clusters obtained by the solvation-desolvation process. *J. Energetic Mater.* **2019**, *37*, 282–292. [CrossRef]
11. Zhao, H.; Gu, G.; Shen, J.; Zhao, X.; Wang, J.; Lan, G. Preparation of Spherical HMX/DMF Solvates, Spherical HMX Particles, and HMX@NTO Composites: A Way to Reduce the Sensitivity of HMX. *ACS Omega* **2023**, *8*, 14041–14046. [CrossRef] [PubMed]
12. Du, Y.-H.; Liu, F.-S.; Liu, Q.-J.; Tang, B.; Zhong, M.; Zhang, M.-J. HMX/NMP cocrystal explosive: First-principles calculations. *J. Mol. Model.* **2021**, *27*, 254. [CrossRef] [PubMed]
13. Duan, X.; Yu, H.; Jie, C.; Li, H. Theoretical Investigation on Structure and Intermolecular Interaction for HMX/DMF Solvate. *Chin. J. Energetic Mater.* **2012**, *20*, 454–458.
14. Landenberger, K.B.; Matzger, A.J. Cocrystals of 1,3,5,7-Tetranitro-1,3,5,7-tetrazacyclooctane (HMX). *Cryst. Growth Des.* **2012**, *12*, 3603–3609. [CrossRef]
15. Mäki-Arvela, P.; Shcherban, N.; Lozachmeur, C.; Eränen, K.; Aho, A.; Smeds, A.; Kumar, N.; Peltonen, J.; Peurla, M.; Russo, V.; et al. Aldol Condensation of Cyclopentanone with Valeraldehyde Over Metal Oxides. *Catal. Lett.* **2019**, *149*, 1383–1395. [CrossRef]
16. Xiao-Hong, L.; Feng-Qi, Z.; Si-Yu, X.; Xue-Hai, J. Molecular dynamics simulation on miscibility of trans-1,4,5,8-tetranitro-1,4,5,8 -tetraazadecalin (TNAD) with some propellants. *J. Mol. Model.* **2013**, *19*, 2391–2397. [CrossRef] [PubMed]
17. Chen, X.; He, L.; Li, X.; Zhou, Z.; Ren, Z. Molecular Simulation Studies on the Growth Process and Properties of Ammonium Dinitramide Crystal. *J. Phys. Chem. C* **2019**, *123*, 10940–10948. [CrossRef]
18. Wu, H.; Zhang, Y.; Chang, P.; Hao, H.; Zhai, L.; Wang, B. Solubility, dissolution properties and molecular dynamic simulation of 2,6-bis(picrylamino)-3,5-dinitropyridine in pure and binary solvents. *J. Mol. Liq.* **2022**, *368*, 120567. [CrossRef]
19. Kilday, M. Enthalpy of Solution of SRM 1655 (KCl) in H_2O. *J. Res. Natl. Bur. Stand.* **1980**, *85*, 467–481. [CrossRef]
20. Chai, J.D.; Head-Gordon, M. Long-Range Corrected Double-Hybrid Density Functionals. *J. Chem. Phys.* **2009**, *131*, 174105. [CrossRef]
21. Boys, S.F.; Bernardi, F. The calculation of small molecular interactions by the differences of separate total energies. Some procedures with reduced errors. *Mol. Phys.* **2002**, *19*, 553–566. [CrossRef]
22. Frisch, M.J.; Trucks, G.W.; Schlegel, H.B.; Scuseria, G.E.; Robb, M.A.; Cheeseman, J.R.; Scalmani, G.; Barone, V.; Petersson, G.A.; Nakatsuji, H.; et al. *Gaussian 09, Revision A.02*; Gaussian, Inc.: Wallingford, CT, USA, 2016.
23. *Materials Studio 2018*, Accelrys Inc.: San Diego, CA, USA, 2017.
24. Xue, L.; Zhao, F.; Xing, X.; Zhou, Z.; Wang, K.; Xu, S.; Yi, J.; Hu, R. Dissolution Thermodynamics of 1,2,3-Triazole Nitrate in Water. *J. Solut. Chem.* **2012**, *41*, 17–24. [CrossRef]
25. Gao, H.-X.; Zhao, F.-Q.; Hu, R.-Z.; Pan, Q.; Wang, B.-Z.; Yang, X.-W.; Gao, Y.; Gao, S.-L. Thermochemical Properties, Thermal Behavior and Decomposition Mechanism of 1,1-Diamino-2,2-dinitroethylene (DADE). *Chin. J. Chem.* **2006**, *24*, 177–181. [CrossRef]
26. Xing, X.L.; Xue, L.; Zhao, F.Q.; Gao, H.X.; Hu, R.Z. Thermochemical properties of 1,1-diamino-2,2-dinitroethylene (FOX-7) in dimethyl sulfoxide (DMSO). *Thermochim. Acta* **2009**, *491*, 35–38. [CrossRef]
27. Hu, R.Z.; Gao, S.L.; Zhao, F.Q.; Shi, Q.Z.; Zhang, T.L.; Zhang, J.G. *Thermal Analysis Kinetics*, 2nd ed.; Science Press: Beijing, China, 2008.
28. Kolker, A.; Safonova, L. Molar heat capacities of the (water + acetonitrile) mixtures at T = (283.15, 298.15, 313.15, and 328.15) K. *J. Chem. Thermodyn.* **2010**, *42*, 1209–1212. [CrossRef]
29. Miller, G.R.; Garroway, A.N. *A Review of the Crystal Structures of Common Explosives*; Part I: RDX, HMX, TNT, PETN, and Tetryl; Naval Research Laboratory: Washington, DC, USA, 2001.
30. Ravindran, T.R.; Rajan, R.; Venkatesan, V. Review of Phase Transformations in Energetic Materials as a Function of Pressure and Temperature. *J. Phys. Chem. C* **2019**, *123*, 29067–29085. [CrossRef]